

①

SILICIDE FORMATION AND SCHOTTKY BARRIER  
OF RARE-EARTH METALS ON SI

Semi-Annual Technical Report

ADA131749

Reporting Period: July 1st, 1982 - December 31st, 1982

Principal Investigator: S. S. Lau

Telephone: (619) 452-3097

Sponsored by: Defense Advanced Research Projects Agency  
DARPA Order No. 3011-4276

Contract No: MDA 903-81-C-0348

Effective: September 30th, 1983

Contractor: University of California, San Diego  
Office of Contract and Grant Administration  
Q-023  
La Jolla  
California 92093

APPROVED FOR PUBLIC RELEASE  
DISTRIBUTION UNLIMITED

DTIC  
SELECTED  
S AUG 25 1983  
A

83 08 23 117

## Table of Contents

	<u>Page</u>
Introduction	1
Summary of Recent Results	2
Summary of Appended Papers	3
Appendix A	4
Appendix B	33

## Introduction

During this period, our activities included the following:

(1) The arrival of the General Ionex Tandetron accelerator. We are now setting this machine up for backscattering experiments. We expect to be on-line in a few months.)

(2) Perfecting the technique of fabricating pit-free  $\text{ErSi}_2$  diodes.

(3) Measurement of barrier heights of Er and  $\text{ErSi}_2$  on p and n type Si. For p-type Si the measurements were done at room temperature. For n-type Si, the measurements were done at 77°K. *degrees*

(4) Presentation of an invited paper entitled "Ion Mixing and Phase Diagrams" at the international conference on Ion Beam Modification of Materials, Grenoble, France, August 1982 (see Appendix A). This paper was written in collaboration with Caltech (B. X. Liu and M-A. Nicolet).

(5) Presentation of a paper entitled "Surface Morphology and Electronic Properties of Erbium Silicide" at the annual MRS meeting held in Boston, November 1982 (see Appendix B).



Accession For	
NTIS GRA&I	<input checked="" type="checkbox"/>
DTIC TAB	<input type="checkbox"/>
Unannounced	<input type="checkbox"/>
Justification	
By _____	
Distribution/	
Availability Codes	
Dist	Avail and/or Special
A	

## Summary of Recent Results

- (1) The barrier height,  $\phi_B^p$ , of Er (before silicide formation) on p-Si has been determined to be  $0.68 \pm 0.01$  eV by I-V measurements at room temperature. The Er layer is laterally uniform before silicide reaction.
- (2) Pitting in the ErSi layer can be completely eliminated by using a sample configuration of Si(a)/Er/Si(xtal). The amorphous Si layer on top also helps in reducing surface oxidation during silicide formation.
- (3) The barrier height,  $\phi_B^p$ , of ErSi<sub>2</sub> on p-Si has been determined to be  $0.76 \pm 0.2$  eV for diodes without surface pits, and  $0.70 \pm 0.2$  eV for diodes with surface pits. The details are presented in appended paper B.
- (4) We have made preliminary  $\phi_B^n$  measurements on n-type Si at 77°K. Barrier heights of Er and ErSi<sub>2</sub> are found to be  $\sim 0.38$  eV and  $\sim 0.30$  eV, respectively.
- (5) The reverse characteristics are much better for pit-free diodes than those with pits (for both n- and p-type Si).
- (6) We face difficulties in growing good quality SiO<sub>2</sub> on p-Si for passivation. The region in Si below the SiO<sub>2</sub> layer is always inverted. We now attempt to form channel stoppers by ion implantation and/or diffusion.
- (7) In spite of these difficulties, we believe we will be able to fabricate devices which are fully passivated and with a guard ring structure for photo-response measurements (in collaboration with Hanscom AFB).

## Summary of Appended Papers

### A. Ion Mixing and Phase Diagrams

This paper reviews the general correlations between the phenomenon of ion mixing which is generally considered to be a non-equilibrium process and binary phase diagrams which are determined by phase equilibria. As it turns out, a number of interactions induced by ion mixing can be predicted by inspecting the binary phase diagram in question. Due to these correlations it appears that the phenomenon of ion mixing can be looked upon from a thermodynamical point of view rather than from a collisional point of view as traditionally practised.

### B. Surface Morphology and Electronic Properties of Erbium Silicide

This paper describes a novel technique to form pit-free  $\text{ErSi}_2$  layers. The concept here is to utilize the fast reaction kinetics between Er and amorphous Si, the resulting  $\text{ErSi}_2$  is pit-free as opposed to heavily pitted  $\text{ErSi}_2$  formed between Er and single crystalline Si substrate. The electronic properties as well as the optimization of these properties of  $\text{ErSi}_2$  diodes on p-type Si are reported. Pit-free  $\text{ErSi}_2$  diodes are shown to be superior in performance as compared to heavily pitted diodes.

ION MIXING AND PHASE DIAGRAMS

S. S. Lau<sup>a)</sup>, B. X. Liu<sup>b)\*</sup>, and M-A. Nicolet<sup>b)</sup>

- a) University of California at San Diego, La Jolla, California 92093, U.S.A.
- b) California Institute of Technology, Pasadena, California 91125, U.S.A.

Interactions induced by ion irradiation are generally considered to be non-equilibrium processes, whereas phase diagrams are determined by phase equilibria. These two entities are seemingly unrelated. However, if one assumes that quasi-equilibrium conditions prevail after the prompt events, subsequent reactions are driven toward equilibrium by thermodynamical forces. Under this assumption, ion-induced reactions are related to equilibrium and therefore to phase diagrams. This relationship can be seen in the similarity that exists in thin films between reactions induced by ion irradiation and reactions induced by thermal annealing. In the latter case, phase diagrams have been used to predict the phase sequence of stable compound formation, notably so in cases of silicide formation.

Ion-induced mixing not only can lead to stable compound formation, but also to metastable alloy formation. In some metal-metal systems, terminal solubilities can be greatly extended by ion mixing. In other cases, where the two constituents of the system have different crystal structures, extension of terminal solubility from both sides of the phase-diagram eventually becomes structurally incompatible and a glassy (amorphous) mixture can form. The composition range where this bifurcation is likely to occur is in the two-phase regions of the phase diagram. These concepts are potentially useful guides in selecting metal pairs that form metallic glasses by ion mixing. In this report, phenomenological correlation between stable (and metastable) phase formation and phase diagram is discussed in terms of recent experimental data.

\*Permanent Address: Peking University, Beijing, The People's Republic of China.

## I. Introduction

When an ion impinges on a target, a sequence of ballistic collisions is initiated by the penetrating ion. This initial part of the process has been referred to as the prompt phase of ion mixing and lasts about  $10^{-12}$  sec. As the energy of the primary particle is distributed over a progressively larger number of atoms, one reaches a state where an average local energy or temperature may be defined. During the prompt event period, the displacement of atoms is presumed to be largely random, so that a correlation between ion-induced mixing of two chemically distinct species and their phase diagram is not expected. As the relaxation process proceeds, a quasi-equilibrium condition may exist locally. If phase diagrams were to be pertinent in this regime, one would expect that they should be diagrams for high pressures, on account of the confinement exerted by the surrounding material. After further relaxation of the excited regions, atoms and defects move toward a configuration that is even closer to thermal equilibrium. The temperature and pressure eventually reach conditions near those of commonly available phase diagrams. In this region a correlation with available phase diagrams may be expected.

Along the path toward equilibrium, metastable states may exist where atoms can be arrested. Without sufficient thermal energy to provide mobility, the system may be frozen in these metastable states and form metastable phases. If a correlation between ion-induced reactions and phase diagrams exists, it appears, then, that this correlation should result from effects that take place during the relaxation of the system after the primary impact (delayed effects).

In the following, we shall examine if indeed there is experimental evidence to indicate that ion-induced reactions between two elements can be correlated to the commonly available binary phase diagrams of the system in question.

## II. Sample Configuration for Ion Mixing Experiments

In general, three types of sample configurations have been used to investigate ion mixing: (1) bilayered samples, where a thin film is deposited onto a substrate. At the early stages of ion irradiation, there is basically an unlimited supply of the top layer material and of the substrate material to interact and form a mixture. Under the conditions of unlimited supply of both components, there is a possibility for the mixed region to seek a preferred composition during the delayed phase of the mixing process; (2) multilayered samples, where interposing thin films ( $\leq 100 \text{ \AA}$ ) of component A and B are deposited onto an inert substrate (e.g.  $\text{SiO}_2$  or sapphire). The average and final composition of the sample in this case is fixed, barring sputtering effects. These samples are sometimes referred to as having a limited supply configuration; (3) thin marker samples, where a very thin marker ( $\leq 10 \text{ \AA}$ ) is imbedded in a matrix of host atoms. The first type of samples (bilayered, unlimited supply) are usually used to compare ion-induced reactions with thin-film reactions that proceed under steady-state annealing conditions. The second type of samples (multilayered, limited supply) are usually used to investigate metastable and amorphous phase formation of a given composition. The third type of samples (thin marker) are used to investigate the basic aspects of ion mixing.

The presently accepted view is that for significant mixing to occur at a given interface, the ions must have sufficient energy to penetrate that interface.

### III. The Q-Curve

In ion mixing experiments, it is often observed, especially in compound forming systems, that the amount of intermixing has two relatively distinct temperature regimes. At low irradiation temperatures, the mixing is insensitive to temperatures; above a certain transition temperature,  $T_c$ , the amount of mixing increases exponentially with temperature [1,2]. This type of temperature dependence is particularly convenient to observe in bilayered (unlimited supply) samples, and is schematically shown in Fig. 1 (commonly referred to as a Q-curve). This behavior can be interpreted as follows: at low temperatures, the mixing is dominated by ballistic processes which depend mainly on the energy and mass of the colliding atoms. These processes are temperature insensitive. Atomic distributions that are nonuniform as a function of distance from the interface are typical for this mixing process. In the high temperature regime, the displaced atoms have enough mobility and time to migrate and relax into a lower free energy configuration as a result of a chemical driving force. In this temperature regime, constant atomic concentration profiles are often observed at the interface. Distinct compounds (if present in the phase diagram) form there due to ion mixing. Although most of the samples are analyzed at room temperature hours after ion irradiation, it is believed that the low temperature-mixed layers do not typically relax significantly

upon warming to room temperature and that the results are thus typical of atomic distributions that have been extremely rapidly quenched. On the other hand, the high temperature-mixed layers relax substantially due to delayed effects. Since relaxation leads to equilibrium, a correlation between ion mixing and phase diagrams should be strongest in the thermally activated regime of the Q-curve.

The majority of the systems for which Q-curves have been measured so far are transition metal/Si systems[1,2,3]. The value of the transition temperature,  $T_c$ , depends on the system, but is typically around room temperature. The details of the Q-curve, such as the temperature-independent Q value and the activation energy in the thermally activated regime, also depend on the systems considered and on the irradiation conditions. Very few metal-metal systems have been investigated so far, but the available evidence[4,5,6] seems to conform to the general behavior of the Q-curves found for transition metal/Si system. To gain a general picture, additional experimental results on metal-metal systems are very much needed.

#### IV. Correlation Between Steady-State Annealing and Ion Mixing

The formation of equilibrium compounds by ion mixing at room temperature has been investigated rather extensively in silicide forming systems using bilayered structures. The results are tabulated in Table I. The ion-induced silicide formation characteristics can be compared with those obtained by thermal steady-state annealing. The results of silicide formation by thermal annealing are well-documented[7] and summarized in Table I also. It can be clearly seen from Table I that the first silicide phase induced by

ion mixing in unlimited supply samples is the same as that obtained by thermal annealing. Although some of the layers that were ion mixed at R.T. do not exhibit a distinct crystal structure due to weak x-ray diffraction patterns, the composition of the mixed layer deduced by backscattering is invariably the same as that obtained by thermal annealing. As the temperature of irradiation is increased to above R.T., the crystal structure of the phase can be identified even in those cases as being the same as that obtained by thermal annealing[8,9]. If we assume that ion mixing at room temperature is in the thermally activated regime of the Q-curve for all systems studied, we can conclude that there is a direct one-to-one correlation between thermal annealing and ion-mixing in the thermally activated regime, at least in silicide forming systems. This being so, searching for a correlation between ion mixing and phase diagrams amounts to correlating the silicide formation by thermal annealing to phase diagrams. Such a correlation has indeed been established.

The correlation between the first silicide phase observed upon thermal annealing of a bilayer sample and the phase diagram was first proposed by Walser and Bené[10]. Their rule states that the first silicide to grow upon thermal annealing of a bilayered sample is the highest congruently melting compound next to the lowest-melting eutectic in the phase diagram (for example,  $\text{Ni}_2\text{Si}$  in the Ni-Si system, or  $\text{Pd}_2\text{Si}$  in the Pd-Si system). This correlation is about 80-90% accurate in predicting the first phase[7]. Based on this correlation, we can thus state that the first phase induced by ion mixing in unlimited supply samples is the highest congruently melting compound next to the lowest eutectic in the phase diagram, provided

that ion mixing is performed in the thermally activated regime of the Q-curve.

Although this rule is quite successful in correlating ion-induced silicide formation with phase diagrams, it is not clear if such a correlation also exists in bilayered metal-metal systems. Few ion mixing experiments have so far been performed on metallic bilayers. Furthermore, thermal annealing of such samples frequently induces laterally nonuniform reactions[11]. More work is required in this area to clarify the issue.

#### V. Amorphous Alloy Formation and Phase Diagrams

It has long been recognized that alloys having compositions near deep eutectics in a binary phase diagram have enhanced glass-forming ability by quenching techniques[12,13]. This type of phase diagram is schematically illustrated in Fig. 2, where the A-rich side of the A-B diagram is shown. When ideal solution theory is applied to calculate the liquidus curve, the dashed line results. Experimentally, however, the liquidus curve bends down to much lower temperatures around the eutectic composition (see Fig. 2). This deviation from ideal solution behavior is explained in terms of enthalpy of mixing  $\Delta H_m$  of the system, with  $\Delta H_m^S$  (heat of mixing in the solid solution)  $>$   $\Delta H_m^L$  (heat of mixing in the liquid solution)[14]. Since  $\Delta H_m^S$  is larger than  $\Delta H_m^L$ , it is possible that the structure of the eutectic liquid near the eutectic temperature consists of two distinct types of clusters which are microscopically bifurcated into local regions with dimensions of a few atomic distances. In the

eutectic liquid just above the eutectic temperature, one might expect to find that A-rich regions have the short range order of solid A interspersed with B-rich regions having the short range order of solid B. The atoms surrounding these two types of local regions are considered to be liquid-like and to retain a substantial entropy of mixing, provided that the cluster size is not too large. A competition exists between entropy of mixing (which favors small clusters) and enthalpy gained by bifurcation (which favors large clusters). A balance between these two factors to minimize the free energy of the system will determine the optimum size of the clusters. If this bifurcated liquid is rapidly quenched below the glass transition temperature,  $T_g$ , a glassy alloy will be produced.

Previous experimental investigations on ion-induced reactions using multi-layered samples (limited supply) showed that ion mixing is well-suited for metastable phase formation in metal-metal systems [1,15]. In particular, when the two components of the binary system have the same crystalline structure, but exhibit a miscibility gap in the phase diagram, supersaturated solid solutions are obtained upon ion mixing. This situation is illustrated in Fig. 3. A schematic phase diagram of a simple eutectic system is shown in the upper portion of Fig. 3, where the two components have the same crystal structure (for example, Ag-Cu, f.c.c. structure). The lower portion of Fig. 3 shows the sequence of events upon ion mixing (with, say, Xe ions) of multilayered samples of various compositions. At low-doses (or low dpa numbers), the multiple layers start to intermix, but generally with little or no metastable phase formation. As

doses increase, the miscibility gap is closed and a metastable crystalline phase (MX) with f.c.c. structure is formed across the whole range of the miscibility gap with imperceptible traces of non-crystalline phases. On the other hand, when the crystal structures of the two components are different (say f.c.c. for component A and b.c.c. for component B), a tendency to form amorphous alloys by ion mixing can clearly be detected in the existing literature[1,15].

In view of the bifurcation concept discussed previously for an eutectic liquid, one is led to speculate that ion mixing can be profitably used to produce metallic glasses by judiciously selecting systems with the guidance of binary phase diagrams. In order to bifurcate an alloy, it is desirable to choose a binary system with a deep eutectic located in a two-phase region where the phases on both sides have different crystal structures ( a condition easily met in phase diagrams). This concept was put to test in metal-metal systems using multilayered samples with fixed overall compositions[16]. The binary systems and compositions were chosen according to the following criteria: (1) the two constituent elements have different crystal structures; (2) the composition of the multilayered samples is fixed near a deep eutectic, away from equilibrium compounds or pure metals; (3) some systems were chosen to have almost identical atomic sizes and others to have almost identical electronegativities, but always with different crystal structures. Xenon ions were usually used for irradiation because of the high efficiency in inducing atomic mixing. The full details of this investigation is presented here in this Conference as a contributed paper[16]. The results are summarized

here: It is found that in eight metal-metal binary systems with multilayered sample configuration, irradiation leads to uniform mixing of the interposed layers. An amorphous alloy is formed in every case, irrespective of the atomic size and the electronegativity properties of the constituents, as long as the constituents have different crystal structures. Figure 4 shows a schematical phase diagram with different crystal structures of the elements and the sequence of events as a function of dose (or dpa). Inter-mixing of the two phases is observed at relatively low doses ( $< 2 \times 10^{15}$  Xe/cm<sup>2</sup> or  $< 20$  dpa). For samples with compositions near either A or B, extended solid solutions  $\alpha'$  and  $\beta'$  with structures identical to their parent phases are observed at increasing doses ( $\alpha'$  has the structure of  $\alpha$ ,  $\beta'$  that of  $\beta$ ). As the composition approaches from the A side (f.c.c. or h.c.p.) to the middle of the two-phase region, the mixed layer (20  $\lesssim$  dpa  $\lesssim$  50-100) consists of a mixture of an amorphous phase and a metastable crystalline phase of h.c.p. structure (but with a different c/a ratio compared to that of A if A is also h.c.p.). On the B side, a mixture of an amorphous phase and  $\beta'$  (b.c.c.) is observed in the mixed layer. Increasing the ion dose leads to complete amorphization of the mixed layer in a composition range near the eutectic composition. At even higher doses, the amorphous phase may dissociate into metastable or equilibrium phases, possibly due to ion-beam demixing effects[17].

## VI. Thin Marker Experiments

The effects of ion mixing have been investigated with thin markers in a number of systems [18,19,20,21]. The samples generally consist of a thin layer of impurity ( $\sim 10 \text{ \AA}$ ) imbedded in vacuum-deposited Si. Inert gas ions were irradiated into the sample with a projected range exceeding the location of the thin marker in the matrix. The temperature of implantation ranged from  $\sim 80$  to  $523^\circ\text{K}$ . The mixing phenomenon can be investigated by the spreading (approximated by Gaussian curves) and the shift of the thin marker after irradiation. For this discussion, we shall concentrate on the spreading of the thin markers only. It was found that the spreadings after irradiation at low temperatures for an elemental markers such as Ni, Ge, Sn, Ab, Pt and Au is insensitive to the mass of the marker [19]. This observation is strong evidence that the spreading is due primarily to interactions of the marker atoms with atoms in the matrix, and not with the incident ions themselves. Figure 5 shows  $1.5 \text{ MeV } ^4\text{He}^+$  backscattering spectra for a Sn marker before and after irradiation with  $1 \times 10^{16} \text{ Kr}^+/\text{cm}^2$  of  $220 \text{ keV}$  in the temperature-independent regime [19]. As the irradiation temperature is increased to room temperature or above, marker elements that do not form silicides (such as Ge, Sn, Sb and Au) exhibit Gaussian profiles up to  $\sim 523^\circ\text{K}$ . On the other hand, elements that form silicides (Ni, Pd and Pt) exhibit non-Gaussian profiles, suggesting a reduction in the efficiency of mixing compared to that obtained at low temperature (see Fig. 6). This non-Gaussian profile can be approximated by two superimposed Gaussian profiles: one whose

standard deviation is broadened by the irradiation, and another profile that is altered little. These mixing characteristics of silicide forming elemental markers (two Gaussians or reduction in efficiency in mixing) can be interpreted as the result of some compound formation. A hypothetical scenario is that the effect of the prompt ballistic mixing is to initially spread the thin marker. However, if the chemical driving force is strong enough and atomic mobilities are sufficient, a compound may form during the relaxation period of the impact (delayed processes). The spreading may consequently be much reduced as a thin layer of silicide would form with portions of the marker atoms. Although the exact nature of the non-Gaussian behavior requires further clarification, particularly with TEM, these marker experiments offer ample evidence that compound formation (hence phase diagram) plays a role in ion mixing.

As the thickness of a silicide forming thin marker increases, the mixing efficiency is observed to increase as well. For a Pt marker in Si, at a dose of  $2 \times 10^{16}$  Xe/cm<sup>2</sup> at 300 keV and room temperature, the effective diffusion length,  $\sqrt{Dt}$  is 90 Å for a 5 Å Pt marker, as compared to 180 Å for a 30 Å Pt marker in Si [18,19]. As the Pt increases further to a bilayer configuration, an even thicker Pt<sub>2</sub>Si is formed after a relatively low dose of  $\sim 10^{15}$  Xe/cm<sup>2</sup>. This observation again indicates the importance of thermodynamical forces in ion mixing.

The influence of chemical forces is also evident in cases where ion mixing is observed to be very reduced. It has been observed that binary systems with very limited mutual solubility

in both the solid and the liquid phase (e.g. Cu-W, Ag-Ni) show very little change upon irradiation as compared to other binary systems<sup>4</sup>[22].

#### VII. Summary Remarks

When faced with a binary phase diagram, we can at this time venture some guesses on the characteristics of ion mixing of the system upon inspection of the phase diagram:

- 1) For completely immiscible systems (for example, Cu-W), ion irradiation does not tend to cause significant intermixing, even if the samples are composed of thin interposed layers.
- 2) In systems that form compounds or solid solutions, ion irradiation causes efficient intermixing.
- 3) For transition metal-Si systems and unlimited supply samples, the first phase induced by ion mixing is the same as that obtained by steady-state annealing. Since the first phase formed by thermal annealing is related to the phase diagram via the Walser-Bené rule, the same rule applies to ion mixing of transition-metal silicides.
- 4) For metal-metal systems and limited supply samples, if the two constituents of the system have the same crystal structure, much extended solubility from either side of the phase diagram is generally expected.
- 5) For metal-metal systems and limited supply samples, if the two constituents of the system have different crystal structures, an amorphous alloy is obtained upon ion mixing.

If a deep eutectic is present between a two-phase region in the phase diagram, the glass forming ability of the system is expected to increase for samples with compositions near the eutectic.

- 6) For thin marker samples where a thin impurity layer is imbedded in a Si matrix, the spreading of silicide forming markers at room temperature is non-Gaussian, suggesting that phase formation may occur upon ion mixing, whereas non-compound forming markers exhibit Gaussian profiles after ion mixing.

Although the correlation between phase diagrams and ion mixing is evident, there are many unanswered questions. For example:

- 1) For the case of metal-metal systems and unlimited supply samples case, the phase induced by ion mixing is not always the same as that obtained by thermal annealing. There are only a few metal-metal systems investigated, and only one system (Ni/Al) [1] gives the same phase by either ion mixing or thermal annealing. An extensive and systematic study of metal-metal systems are needed.
- 2) For the case of metal-metal systems and limited supply samples, no compound formation has been detected even at very low doses although phase diagrams indicate the presence of phases. As the dose increases, either solid solution forms or amorphous alloy is obtained, depending on the crystal structure of the constituents. It is not clear at present why equilibrium phases are not observed by ion mixing in limited supply cases.

- 3) Certain simple eutectic systems such as Ge-Au[31] and Si-Au[31] mix efficiently and uniformly, however, others such as Si-Ag[31,32] and Ge-Al[31] tend not to mix. All four systems have very similar phase diagrams. Therefore, the difference in mixing characteristics cannot always be interpreted in terms of phase diagrams.
- 4) In the formation of amorphous phase, there is no clear picture of how bifurcation takes place (if at all) during ion mixing. The basic issue is how to model the ion mixing process and the subsequent relaxation in the delayed regime. Quite evidently, much more work is needed to put the correlation between ion mixing and phase diagrams on a solid basis.

#### Acknowledgment

The authors thank Dr. William L. Johnson for interesting discussions, R. Fernández, for assistance in the preparation of samples. This work was executed under the benevolent U. R. Fund of the Böhmische Physical Society (B. M. Ullrich). The irradiation part of the study was financially supported in part by the U.S. Department of Energy through an agreement with the National Aeronautics and Space Administration and monitored by the Jet Propulsion Laboratory, California Institute of Technology (D. B. Bickler), at the California Institute of Technology; and by the Defense Advanced Research Project Agency (S. Roosild), at the University of California, San Diego, La Jolla, California.

References

- [1]. J. W. Mayer, B. Y. Tsaur, S. S. Lau, and L.-S. Hung,  
Nucl. Instr. Meth. 182/183 (1981) 1.
- [2]. R. S. Averback, L. J. Thompson, Jr., J. Moyle, and  
M. Schalit, J. Appl. Phys. 53 (1982) 1342.
- [3]. B. Y. Tsaur, in Proceedings of the Symposium on Thin Film  
Interfaces and Interactions, J. E. E. Baglin and J. M. Poate,  
Eds., (The Electrochemical Society, Princeton, 1980),  
Vol. 80-2, p. 205.
- [4]. Z. L. Wang, J. F. M. Westendorp, S. Doorn, and F. W. Saris,  
in Metastable Materials Formation by Ion Implantation, S. T.  
Picraux and W. J. Choyke, Eds., (North-Holland, New York, 1982),  
MRS Symposia Proceedings Vol. 7, p. 59.
- [5]. S. T. Picraux, D. M. Follstaedt, and J. Delafond, in Metastable  
Materials Formation by Ion Implantation, S. T. Picraux and  
W. J. Choyke, Eds., (North-Holland, New York, 1982), MRS  
Symposia Proceedings Vol. 7, p. 71.
- [6]. B. M. Paine, M-A. Nicolet, and T. C. Banwell, in Metastable  
Materials Formation by Ion Implantation, S. T. Picraux and  
W. J. Choyke, Eds., (North-Holland, New York, 1982), MRS  
Symposia Proceedings Vol. 7, p. 79.
- [7]. M-A. Nicolet and S. S. Lau, "Formation and Characterization  
of Transition Metal Silicides", to be published as a Chapter in  
VLSI ELECTRONICS: MICROSTRUCTURE SCIENCE, N. Einspruch, Series  
Ed., Supplement A - Materials and Process Characterization,  
G. Larrabec, Guest Ed., (Academic Press, New York, in press).

References (continued)

- [8]. S. Matteson, J. Roth, and M-A. Nicolet, *Rad. Effects*, 42 (1979) 217.
- [9]. B. Y. Tsaur, Ph.D. Thesis, California Institute of Technology, 1980.
- [10]. R. Walser and R. Bené, *Appl. Phys. Lett.* 28 (1976) 624.
- [11]. J. E. E. Baglin and J. M. Poate, in Thin Films - Interdiffusion and Reactions, J. M. Poate, K. N. Tu, and J. W. Mayer, Eds., (Wiley, New York, 1978), Chapter 9.
- [12]. W. L. Johnson, in Glassy Metals. I., H. J. Güntherodt and H. Beck, (Springer-Verlag, New York, 1981).
- [13]. W. L. Johnson, in Metastable Materials Formation by Ion Implantation, S. T. Picraux and W. J. Choyke, Eds., (North-Holland, New York, 1982), MRS Symposia Proceedings Vol. 7, p. 18.
- [14]. R. A. Swalin, Thermodynamics of Solids, 2nd Edition, (Wiley, New York, 1972).
- [15]. B. Y. Tsaur, S. S. Lau, L.-S. Hung, and J. W. Mayer, *Nucl. Instr. Meth.* 182/183 (1981) 67.
- [16]. B. X. Liu, W. L. Johnson, M-A. Nicolet, and S. S. Lau, paper in this Conference.
- [17]. B. X. Liu, L. S. Wieluński, M-A. Nicolet, and S. S. Lau, in Metastable Materials Formation by Ion Implantation, S. T. Picraux and W. J. Choyke, Eds., (North-Holland, New York, 1982), MRS Symposia Proceedings Vol. 7, p. 65.
- [18]. B. Y. Tsaur, S. Matteson, G. Chapman, Z. L. Liau, and M-A. Nicolet, *Appl. Phys. Lett.* 35 (1979) 825.

References (continued)

- [19]. S. Matteson, B. M. Paine, M. G. Grimaldi, G. Mezey, and M-A. Nicolet, Nucl. Instr. Meth. 182/183 (1981) 43.
- [20]. S. Matteson, B. M. Paine, and M-A. Nicolet, Nucl. Instr. Meth. 182/183 (1981) 43.
- [21]. B. M. Paine, M-A. Nicolet, R. G. Newcombe, and D. A. Thompson, Nucl. Instr. Meth. 182/183 (1981) 115.
- [22]. T. Banwell (private communication).
- [23]. K. L. Wang, F. Bacon, and . Reihl, J. Vac. Sci. Technol. 16 (1979) 130.
- [24]. B. Y. Tsaur, S. S. Lau, and J. W. Mayer, Appl. Phys. Lett. 35 (1979) 225.
- [25]. B. Y. Tsaur, Z. L. Liau, and J. W. Mayer, Phys. Lett. A71 (1979) 270.
- [26]. T. Kanayama, H. Tanoue, and T. Tsurushima, Appl. Phys. Lett. 35 (1979) 222.
- [27]. W. F. van der Weg, D. Sigurd, and J. W. Mayer, in Applications of Ion Beams to Metals, S. T. Picraux, E. P. EerNisse, and F. L. Vook, Eds., (Plenum Press, New York, 1974), p. 209.
- [28]. G. Chapman, S. S. Lau, S. Matteson, and J. W. Mayer, J. Appl. Phys. 50 (1979) 321.
- [29]. F. M. d'Heurle, M. Y. Tsai, C. S. Petersson, and B. Stritzker, J. Appl. Phys. 53 (1982) 3067.
- [30]. F. M. d'Heurle, C. S. Petersson, and M. Y. Tsai, J. Appl. Phys. (to be published 1982).
- [31]. S. S. Lau, B. Y. Tsaur, M. von Allmen, J. W. Mayer, B. Stritzker C. W. White, and B. R. Appleton, Nucl. Instr. Meth. 182/183 (1981) 97.

References (continued)

- [32]. N. P. Tognetti, R. P. Webb, C. E. Christodoulides, D. G. Armour, and G. Carter, Nucl. Instr. Meth. 182/183 (1981) 107.

Figure Captions

- Figure 1 Schematic Q-curve, where the amount of mixing per incident ion is plotted against the reciprocal absolute temperature of irradiation. This type of mixing behavior is typically observed for bilayered samples of silicide forming systems.
- Figure 2 A schematic A-B phase diagram near the A side.
- Figure 3 Schematic eutectic phase diagram (upper diagram) of two constituents with the same crystal structure (f.c.c.). The lower schematic diagram shows the sequence of events during ion mixing as a function of dose or dpa number (typical values). Only a metastable crystalline phase (MX) is formed in this case. The crystal structure of MX is the same as that of the parent phases.
- Figure 4 Schematic eutectic phase diagram (upper diagram) of two constituents with different crystal structures. The structure of A is either f.c.c. or h.c.p. and the structure B is b.c.c.. The lower diagram shows the sequence of events as a function of dose or dpa number. At medium dose, extended solid solutions ( $\alpha'$  and  $\beta'$ ) are obtained from both sides of the phase diagram. As the composition approaches the middle of the two-phase region from the A side, a mixture of an amorphous phase and a metastable crystalline phase

Figure Captions (continued)

(MX, h.c.p.) is obtained. Approaching the middle of the two-phase region from the B side, a mixture of an amorphous phase and  $\beta'$  is obtained. At higher dose, an amorphous phase is obtained at compositions near the eutectic. The amorphous phase may dissociate upon further irradiation.

Figure 5 1.5 MeV  $^4\text{He}^+$  backscattering spectra of a very thin ( $\sim 10 \text{ \AA}$ ) Sn marker imbedded in an amorphous Si matrix before (a) and after (b) irradiation with 220 keV  $\text{Kr}^+$  ions to a dose of  $1 \times 10^{16}$  ions/cm<sup>2</sup>. The result is typical for irradiation temperatures ranging from 96 to 523°K. The fitted curves are Gaussians [from Ref. 19].

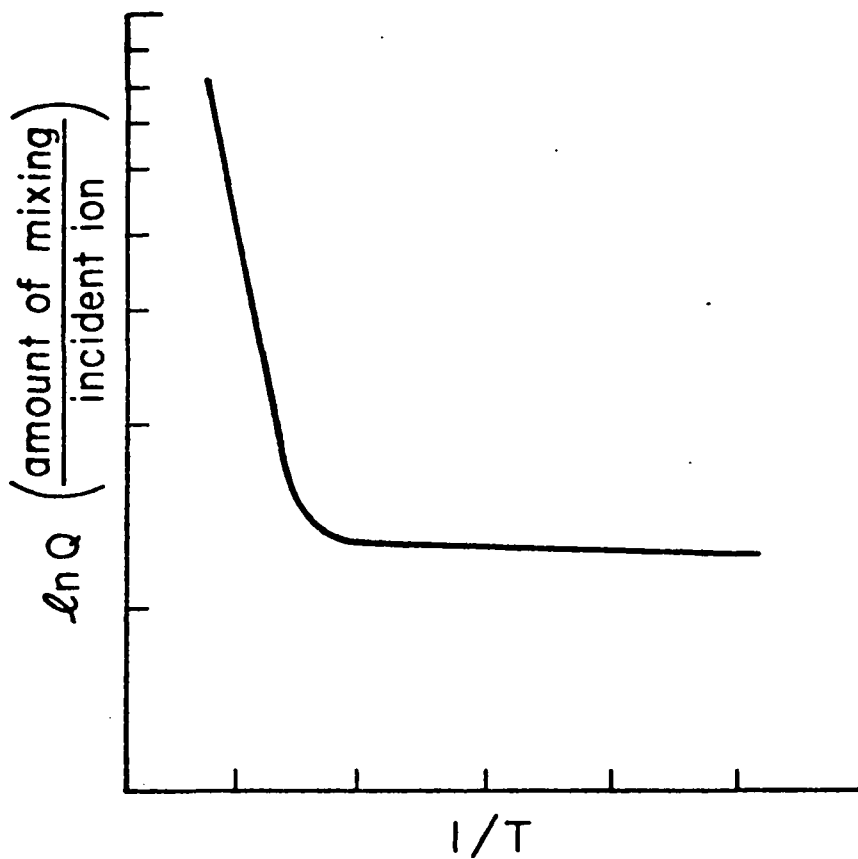
Figure 6 1.5 MeV  $^4\text{He}^+$  backscattering spectra of a very thin ( $\sim 10 \text{ \AA}$ ) Pd marker imbedded in an amorphous Si matrix before (a) and after irradiation (b to d) with 220 keV  $\text{Kr}^+$  ions to a dose of  $1 \times 10^{16}$  ions/cm<sup>2</sup> at three different temperatures. Only the marker signal of the spectrum is shown [from Ref. 19].

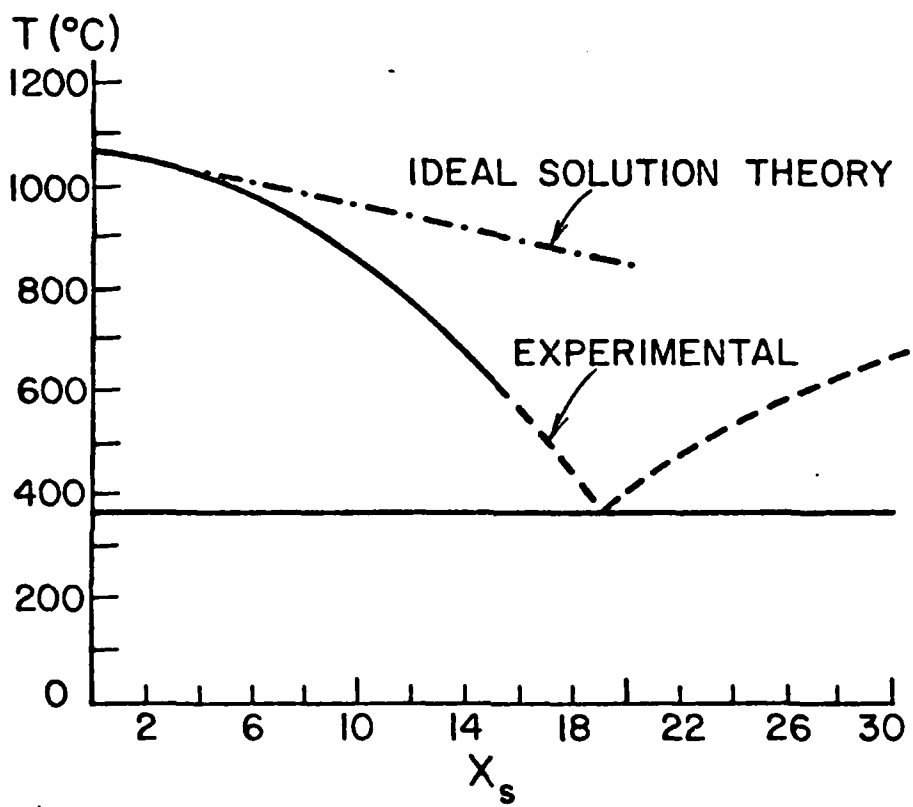
TABLE I. Ion-Induced Interactions in Transition Metal/Si Systems  
(adopted from Ref. [3]).

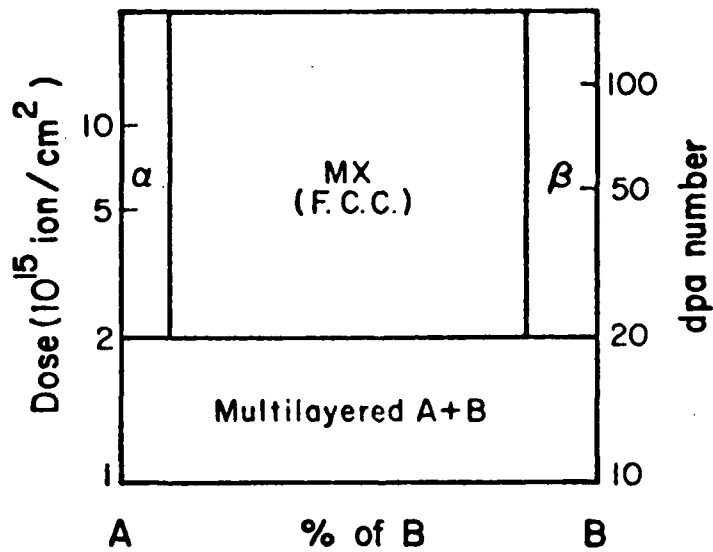
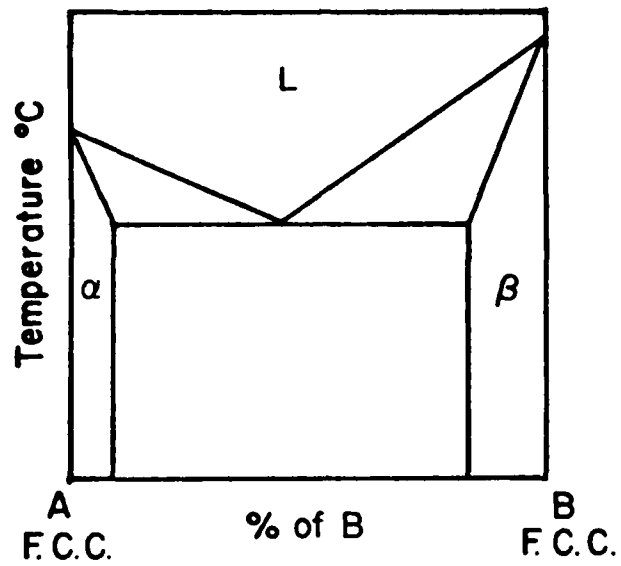
Metal/Si	Ions	Compounds Observed		Phase Formed by Thermal Annealing	Reference
		Composition	Phase		
Ti/Si	N <sup>+</sup> , B <sup>+</sup>	Ti <sub>5</sub> Si <sub>3</sub>	-	TiSi <sub>2</sub>	23
Ti/Si	Ar <sup>+</sup> , Kr <sup>+</sup> , Xe <sup>+</sup>	~TiSi <sub>2</sub>	-	TiSi <sub>2</sub>	3
V/Si	Ar <sup>+</sup> , Kr <sup>+</sup> , Xe <sup>+</sup>	~VSi <sub>2</sub>	-	VSi <sub>2</sub>	3
Cr/Si	Ar <sup>+</sup> , Kr <sup>+</sup> , Xe <sup>+</sup>	~CrSi <sub>2</sub>	-	CrSi <sub>2</sub>	24
Fe/Si	Ar <sup>+</sup> , Kr <sup>+</sup> , Xe <sup>+</sup>	~FeSi	-	FeSi	9
Co/Si	Ar <sup>+</sup> , Kr <sup>+</sup> , Xe <sup>+</sup>	~Co <sub>2</sub> Si	Co <sub>2</sub> Si*	Co <sub>2</sub> Si	9
Ni/Si	Ar <sup>+</sup> , Kr <sup>+</sup> , Xe <sup>+</sup>	Ni <sub>2</sub> Si	Ni <sub>2</sub> Si*	Ni <sub>2</sub> Si	25
Nb/Si	Ar <sup>+</sup>	NbSi <sub>2</sub>	NbSi <sub>2</sub> **	NbSi <sub>2</sub>	26
Nb/Si	Si <sup>+</sup>	NbSi <sub>2</sub>	NbSi <sub>2</sub> <sup>+</sup>	NbSi <sub>2</sub>	8
		Nb <sub>5</sub> Si <sub>3</sub>	Nb <sub>5</sub> Si <sub>3</sub> <sup>++</sup>	NbSi <sub>2</sub>	8
Pd/Si	Ar <sup>+</sup> , Kr <sup>+</sup> , Xe <sup>+</sup>	Pd <sub>2</sub> Si	Pd <sub>3</sub> Si	Pd <sub>2</sub> Si	24, 27, 28
Hf/Si	Ar <sup>+</sup> , Kr <sup>+</sup> , Xe <sup>+</sup>	HfSi	-	HfSi	25
Pt/Si	Ar <sup>+</sup> , Kr <sup>+</sup> , Xe <sup>+</sup>	Pt <sub>2</sub> Si	Pt <sub>2</sub> Si	Pt <sub>2</sub> Si	25
W/Mo/Si	As <sup>+</sup>	WSi <sub>2</sub> /MoSi <sub>2</sub>		WSi <sub>2</sub> /MoSi <sub>2</sub>	29
Mo/Si	As <sup>+</sup> , Ge <sup>+</sup>	MoSi <sub>2</sub>		MoSi <sub>2</sub>	30
Nb/Si	As <sup>+</sup> , Ge <sup>+</sup>	NbSi <sub>2</sub>		NbSi <sub>2</sub>	29

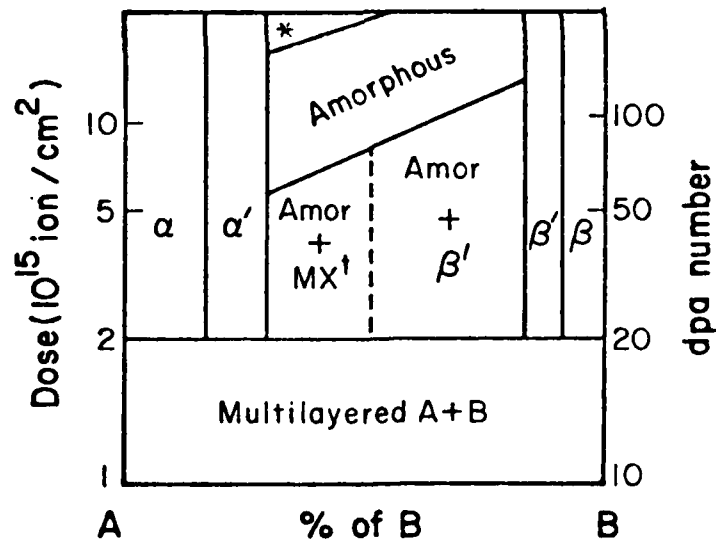
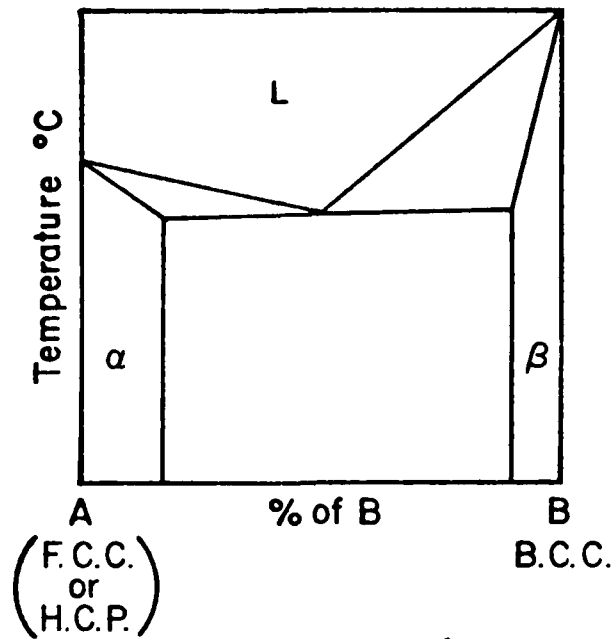
TABLE I.

REMARKS: \* = weak crystalline reflection.  
\*\* = phase observed for samples irradiated at  $\sim 300^{\circ}\text{C}$ .  
- = reflections too weak to be identified.  
† = irradiation temperature  $\sim 300^{\circ}\text{C}$ .  
†† = irradiation temperature  $\sim 113^{\circ}\text{C}$ .



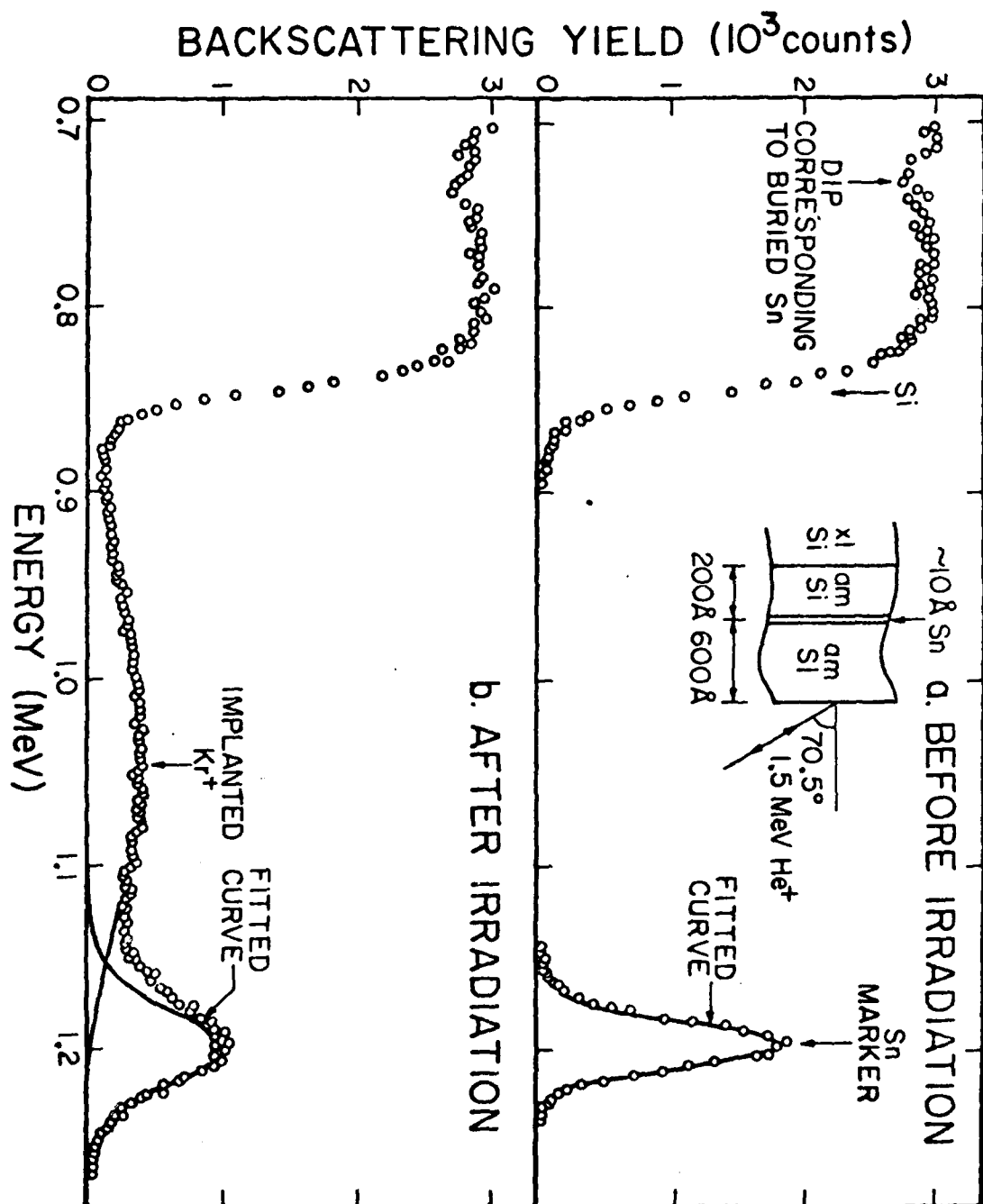


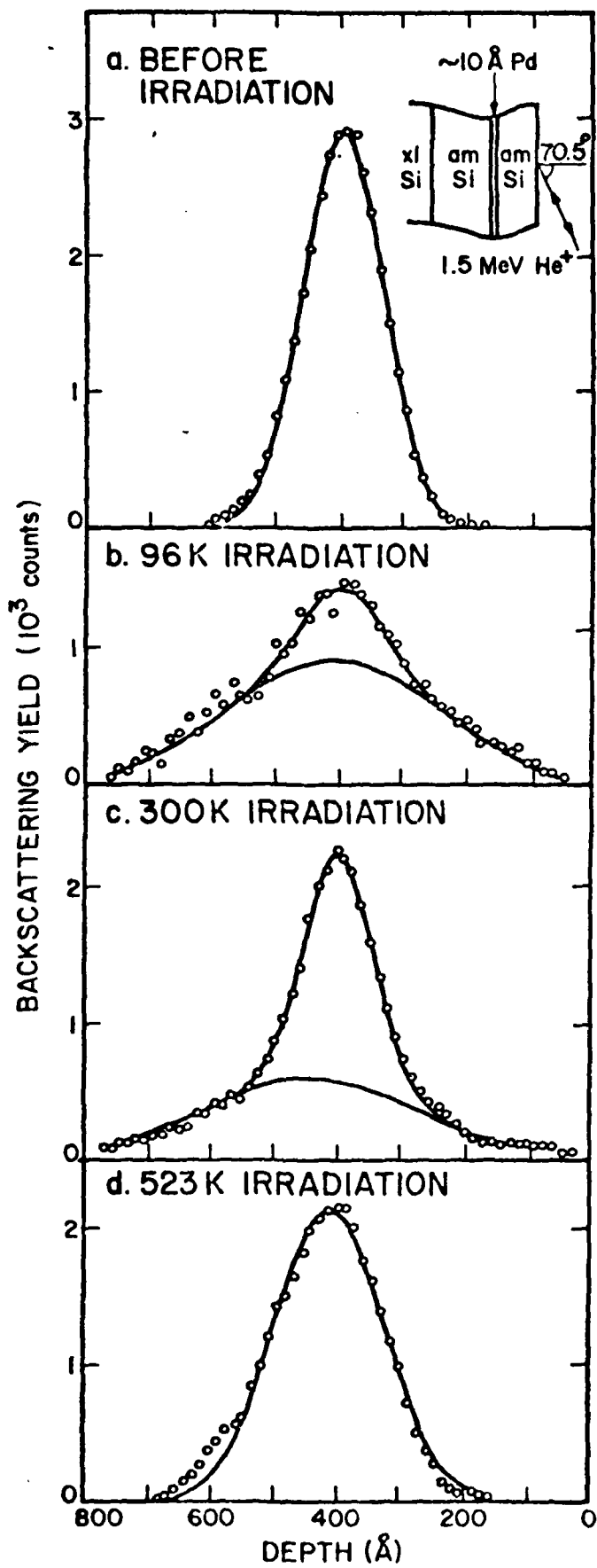




\* sometime amorphous phase dissociates upon relatively high dose irradiation.

† MX is of h.c.p. structure but is different from the H.C.P metal A in size.





Appendix B

Surface morphology and electronic properties of erbium silicide

C. S. Wu, S. S. Lau

Department of Electrical Engineering and Computer Sciences, University  
of California, San Diego, La Jolla, California 92093

T. F. Kuech <sup>(a)</sup> and B. X. Liu <sup>(b)</sup>

California Institute of Technology, Pasadena, California 91125

Abstract

The surface of  $\text{ErSi}_2$ , formed by the reaction of thin Er layers with a single crystal silicon substrate, is typically dominated by deep penetrating, regularly shaped pits. These pits are shown to have detrimental effects on the electronic performance of Schottky barrier height diodes. Surface pits may be reduced in density or eliminated entirely by (i) the use of Si substrate surfaces prepared under ultra-high vacuum conditions prior to metal deposition, or (ii) by means of ion irradiation techniques, or (iii) by reacting Er with an

(a) Present address: IBM Research Center, Yorktown Heights, NY 10598

(b) Permanent address: Quinghua University, Beijing, The People's  
Republic of China

amorphous Si layer. In this investigation, planar  $\text{ErSi}_2$  layers (pit-free) are made using the third approach with a sample structure of  $\text{Si(a)}/\text{Er}/\text{Si}\langle\text{crystal}\rangle$ . The fast reaction between amorphous Si and Er leads to a planar sample structure of  $\text{ErSi}_2/\text{Si}\langle\text{crystal}\rangle$  with little or no reaction between Er and the crystalline Si substrate. The electronic performance of pit-free  $\text{ErSi}_2$  diodes made in this manner is shown to be much superior to those made by reacting Er with Si substrates.

## I. Introduction

The formation of rare-earth metal silicides is characterized by the following observations: (1) the solid state interactions between rare-earth metals (such as Er and Tb) and single crystal Si exhibit a critical temperature phenomenon [1-3]. Below the critical annealing temperature, interactions are very sluggish. Above the critical anneal temperature, interactions are fast, such that within minutes of annealing a layer of rare-earth metal (typically a hundred to a few thousand Å thick) deposited on Si is consumed completely to form a rare-earth metal silicide; (2) Si is found to be the dominant moving species during interactions; (3) the surface morphology of the silicide is typically dominated by a heavy pitting and the pitting is often crystallographic in nature [2]; (4) the surface pits may be reduced in density or eliminated entirely through either the use of Si substrate surfaces prepared under ultra-high vacuum conditions prior to metal deposition and silicide formation or by means of ion implantation techniques. Silicide layers formed by these techniques possess an almost planar morphology [4]; (5) Silicide formation behavior between Er and amorphous Si is distinctly different from that between Er and crystalline Si. Erbium reacts with amorphous Si to form  $\text{ErSi}_2$  in a layer by layer fashion at temperatures as low as  $\sim 300^\circ\text{C}$ , as compared to the critical temperature for reaction observed for crystalline Si ( $\sim 390^\circ\text{C}$ ). The reaction kinetics are observed to be diffusion controlled [5], and the  $\text{ErSi}_2$  layer formed in this manner is laterally uniform without any surface pits [4].

Rare-earth silicides form low Schottky barriers,  $\phi_B^n$ , to n-type Si with  $\phi_B^n \approx 0.3 - 0.4\text{eV}$  [6,7]. This suggests the utility of these Schottky barrier diodes in infrared detecting applications. The presence of surface non-

uniformities, such as surface pitting, could prove to have a detrimental effect on the electronic performance of Schottky barrier devices as well as inaccurate determination of barrier heights by I-V measurements.

The objectives of the present study were to form pit-free  $\text{ErSi}_2$  layers using amorphous Si, without recourse to ion implantation or ultra-high vacuum techniques; and to compare electronic performance of  $\text{ErSi}_2$  diodes with and without surface pitting.

The approach we used to fabricate pit-free  $\text{ErSi}_2$  was to utilize the fast reaction kinetic rate between Er and amorphous Si [4,5]. In this case, a layer of Er was first deposited on a  $\langle 100 \rangle$  Si substrate followed by the deposition of Si on top of the Er layer. A relatively low temperature annealing (300 - 450°C) leads to the formation of pit-free  $\text{ErSi}_2$  between the Er layer and the amorphous Si, without silicide formation between Er and crystalline Si. The situation is schematically shown in Figure 1.

## II. Experimental

Silicon substrates (p-type, 1-10  $\Omega\text{cm}$ ,  $\langle 100 \rangle$  in orientation) were used in this study to facilitate barrier height measurements, ( $\phi_B^p \sim 0.7 - 0.8\text{V}$ ). The wafers were first cleaned by organic solvents, followed by an RCA cleaning process with a final rinse in an HF solution. The wafers were loaded immediately into an ion-pumped vacuum chamber. A layer of Er ( $\sim 500 \text{ \AA}$ ) was deposited onto the substrates, followed by the deposition of Si ( $\sim 750 \text{ \AA}$  n-type 0.002  $\Omega\text{-cm}$ ) on top of the Er layer. The Si layer thickness was chosen such that a layer of  $\text{ErSi}_2$  would form after thermal annealing. The rate of deposition was  $\sim 10 \text{ \AA/sec}$  for Er and 20 - 30  $\text{ \AA/sec}$  for Si, at a pressure of  $\sim 10^{-7}$  torr. A heavily doped n-type Si charge was used for evaporation to increase the conductivity of the deposited Si (amorphous) layer so that electrical measurements could be made before any silicide formation.

For electrical evaluation, diodes with sizes of 0.5 mm, 1 mm and 3 mm in diameter were made on the wafers with mechanical masks. For comparative purposes a similar set of diodes with only Er on p-Si was also made. The samples were analyzed before and after vacuum ( $< 5 \times 10^{-7}$  torr) or flowing forming gas (15%  $\text{H}_2$ , 85%  $\text{N}_2$ ) annealing with x-ray Read Camera and MeV  $^4\text{He}^+$  backscattering techniques. The barrier heights and leakage currents were determined by current voltage measurements.

### III. Results

The surface morphologies of  $\text{ErSi}_2$  layers formed on Si with the conventional method and with the new approach are shown in Figure 1. It can be seen from the optical micrographs that the  $\text{ErSi}_2$  layer formed by reacting Er with amorphous Si on top of Er is much more uniform laterally than that formed by reacting Er with the Si substrate.

The forward and reverse I-V characteristics of these samples before annealing (silicide formation) are shown in Figure 2 (only 3 mm diodes are shown). The barrier heights,  $\phi_B^p$ , of both  $\text{Er/Si}\langle p,100\rangle$  and  $\text{Si(a)/Er/Si}\langle p,100\rangle$  samples are found to be  $0.68 \pm 0.01\text{eV}$  with an n factor of  $\sim 1.05$ , relatively independent of the size of the diodes. Since these diodes have not been passivated, the reverse currents cannot be determined accurately. However, the lowest reverse currents measured at 10 volts are about seven times (7x) higher than the theoretical reverse current, calculated from considering only the effect of image force lowering.

After silicide formation, the barrier heights of both types of samples are observed to increase. Figure 3 shows the I-V characteristics observed on both types of samples after annealing at  $450^\circ\text{C}$  for 30 minutes in forming gas.

The barrier height,  $\phi_B^p$ , of  $\text{ErSi}_2$  diodes formed by reacting Er with Si substrate is found to be  $0.7 \pm 0.02\text{ eV}$  with an n factor of  $\sim 1.1$ . The silicide layer formed on this type of sample ( $\text{Er/Si}\langle 100\rangle$ ) is not laterally uniform as shown in Figure 1. The reverse characteristics show soft break down behavior (see Figure 3). The lowest reverse current measured at 10 V is about 100 times the calculated reverse current. The barrier height,  $\phi_B^p$ , of  $\text{ErSi}_2$  formed by reacting Er with amorphous Si is found to be  $0.76 \pm 0.02\text{eV}$  with an n factor of 1.05. The reverse currents for this type of sample ( $\text{Si(a)/Er/Si}\langle p,100\rangle$ )

after silicide formation are usually much smaller than those observed on Er/Si<100> samples after silicide formation. The lowest reverse current measured at 10 V is about 20 times the calculated reverse current (Figure 3).

It is also found that the barrier heights of both types of samples change as a function of annealing temperature for a given annealing time. This behavior is shown in Figure 4 (for a 30 minute annealing period). For samples with a configuration of Si(a)/Er/Si<p,100>, the barrier height increases from an as-deposited value of  $\sim 0.68$  eV to a maximum of  $\sim 0.77$  eV at  $\sim 380^\circ\text{C}$  and then gradually decreases to 0.74 eV at  $500^\circ\text{C}$ . The initial rise of  $\phi_B^D$  is believed to be due to the reduction of the interfacial oxide and other contaminations, between the Er layer and the Si substrate, by the Er layer without silicide formation, thus allowing intimate contact between Er and the Si substrate. A maximum value of  $\phi_B^D$  is obtained when an  $\text{ErSi}_2$  layer is formed between Er and amorphous Si and is in contact with the Si substrate. The temperature and time ( $380^\circ\text{C}$ , 30 minutes) for this to occur is consistent with reported kinetics [5], and confirmed by backscattering in our case. The reason for the gradual decrease of  $\phi_B^D$  after the maximum is not clear at present. However, this could be due to the very rapid reaction rate between Er and amorphous Si to form silicide at high temperatures, such that the reduction of interfacial oxide could not be completed before the total consumption of Er. For samples with an Er/Si<p,100> configuration,  $\phi_B^D$  increases from 0.68 eV to a maximum of 0.75 eV at  $\sim 350^\circ\text{C}$  and then decreases relatively rapidly to  $\sim 0.68$  eV at  $\sim 500^\circ\text{C}$ . The initial rise of  $\phi_B^D$  can be interpreted as before. The decrease of  $\phi_B^D$  after the maximum is likely to be an effect of silicide formation between Er and the Si substrate. Because of silicide formation, pits begin to form at the  $\text{ErSi}_2/\text{Si}<p,100>$  interface, thus affecting the effective area for current density determination. Shallow

pits are visible after annealing at 380°C for 30 minutes. As the annealing temperature increases, surface pits become more pronounced. The barrier height is observed to decrease rapidly between 400°C and 450°C, corresponding to the appearance of a high density of deep penetrating surface pits.

The effect of annealing time at a given temperature on the barrier height is shown in Figure 5 (380°C annealing). For samples with a Si(a)/Er/Si<p,100> configuration,  $\phi_B^p$  increases with annealing time until it reaches a saturation value ( $\sim 0.77$  eV) after  $\sim 0.4$  hours of annealing. This corresponds to the total consumption of Er to form  $\text{ErSi}_2$  between Er and amorphous Si and the Si substrate is now in contact with a planar  $\text{ErSi}_2$  layer. For samples with an Er/Si<p,100> configuration,  $\phi_B^p$  reaches a saturation value of  $\sim 0.72$  eV after  $\sim 0.1$  hours of annealing. We believe that this is the time necessary to reduce the interfacial oxide by Er at 380°C. Shallow surface pits begin to develop after 30 minutes of annealing. The barrier height remains relatively constant at  $\sim 0.72$  eV even after 10 hours of annealing, although shallow surface pits appear to increase somewhat after longer periods of annealing. The electrical properties of Er silicide diodes formed on both types of samples are briefly summarized in Table 1.

#### IV. Discussion and Summary

The effects of lateral non-uniformity of  $\text{ErSi}_2$  layers can be clearly seen by the lowered barrier heights and increased reverse currents (see Figures 1 and 3). These observations can be explained by an increased effective area of diodes for current transport and high electric fields associated with pits in the  $\text{ErSi}_2$  layer. Using a sample configuration of  $\text{Si(a)}/\text{Er}/\text{Si}\langle\text{xtal}\rangle$ , laterally uniform  $\text{ErSi}_2$  layers can be formed on single crystal Si substrates. This approach takes advantage of the fact that Er reacts with amorphous Si at temperatures much lower than the critical temperature above which Er reacts with single crystal Si rapidly. Diodes of  $\text{ErSi}_2$  with a planar structure are shown to have higher barrier heights and much reduced reverse currents. At temperatures below the critical temperature, the reaction between Er and single crystal Si to  $\text{ErSi}_2$  is sluggish, however, we suggest that the Er layer can reduce the native oxide layer and other contaminations located at the  $\text{Er}/\text{Si}\langle\text{xtal}\rangle$  interface due to the chemical activity of Er. The reduction of interfacial contamination permits a more intimate contact between Er and the Si surface and leads to increased barrier heights without silicide formation, as shown in the initial rise of  $\phi_B^p$  in Figures 4 and 5. This speculation is supported by the observation that when an HF rinsed Si substrate is backside heated to  $500^\circ\text{C} - 600^\circ\text{C}$  in a vacuum of  $\sim 1 \times 10^{-8}$  torr and then cooled to room temperature before Er deposition, the barrier height of such a sample is  $\sim 0.8$  eV which is much higher than those obtained on samples without backside heating ( $\sim 0.68$  eV). This heating resulted in the desorption of mainly fluorine atoms (originating from HF used on the Si surface), and should lead to a relatively contamination free Si surface [4] (hence the high  $\phi_B^p$  value).

Although high barrier height Schottky diodes of Er on p-Si (hence low barrier heights on n-Si) can be fabricated by proper preparation of the Si

substrate without silicide formation, the elemental Er layer is extremely active and normally oxidizes in room air. Formation of  $\text{ErSi}_2$  improves the stability of these diodes significantly, since  $\text{ErSi}_2$  is stable up to  $800^\circ\text{C}$  and above. Using a sample configuration of  $\text{Si(a)}/\text{Er}/\text{Si}\langle\text{xtal}\rangle$  not only allows the formation of laterally uniform  $\text{ErSi}_2$  layers, but also relaxes the annealing ambient for silicide formation. In fact, functional planar diodes of  $\text{ErSi}_2$  can be obtained by annealing the  $\text{Si(a)}/\text{Er}/\text{Si}\langle 100 \rangle$  structure in air at  $\sim 400^\circ\text{C}$ . This is because the top amorphous Si layer protects the Er layer from oxidation. Once silicide is formed between Er and amorphous Si, the resulting  $\text{ErSi}_2$  layer is stable against oxidation at  $\sim 400^\circ\text{C}$ .

In summary, we have shown that laterally uniform  $\text{ErSi}_2$  layers can be easily formed by a simple method. The barrier heights determined by I-V measurements on pit-free  $\text{ErSi}_2$  diodes are believed to be more accurate. Schottky diodes of  $\text{ErSi}_2$  are stable against oxidation and should prove useful as reliable infrared detectors (on n-type Si).

Acknowledgement

The authors are indebted to R. Fernandez for technical assistance, M. Bartur and M-A. Nicolet (Caltech) for discussion. This work is supported by DARPA (MAA 903-81-C-0348, S. Roosild) at the University of California, San Diego, and by the U.S. Department of Energy through an agreement with the National Aeronautics and Space Administration and monitored by the Jet Propulsion Laboratory at the California Institute of Technology (D. Bickler).

Table 1

Electrical Properties of ErSi<sub>2</sub> Diodes

Sample Configuration	Annealing Condition	Surface Condition	$\phi_B^p$ (eV)	n
Er/Si<p,100>	as-deposited	planar	$0.68 \pm 0.01$	1.05
Er/Si<p,100>	380°C, 60 min* silicide formed	pits	$0.71 \pm 0.02$	1.1
Si(a)/Er/Si<p,100>	as-deposited	planar	$0.68 \pm 0.01$	1.05
Si(a)/Er/Si<p,100>	380°C, 30 min* silicide formed	planar	$0.78 \pm 0.02$	1.05

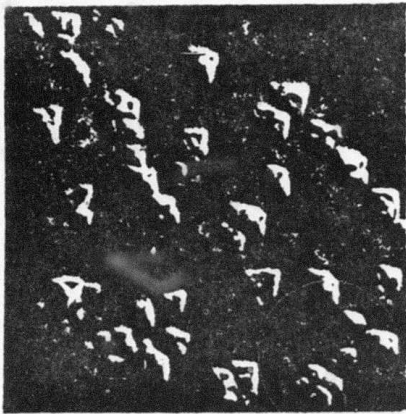
\* annealing condition for achieving maximum barrier heights

## References

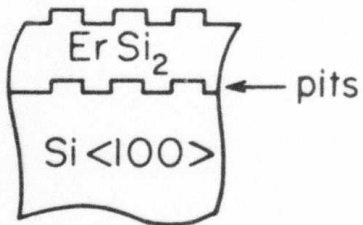
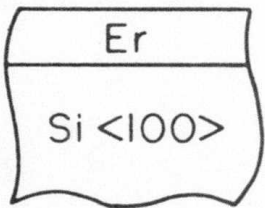
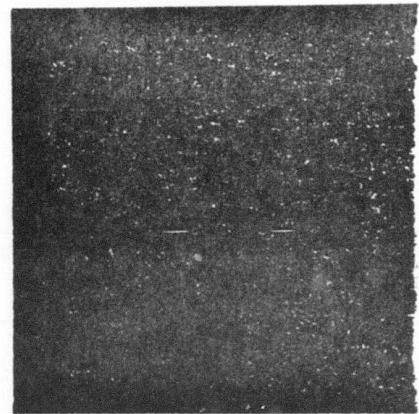
1. J. E. E. Baglin, F. M. d'Heurle and C. S. Petersson, Appl. Phys. Lett. 36, 594 (1980).
2. R. D. Thompson, B. Y. Tsaur and K. N. Tu, Appl. Phys. Lett. 52, 2841 (1981).
3. J. E. E. Baglin, F. M. d'Heurle and C. S. Petersson, J. Appl. Phys. 52, 2841 (1981).
4. S. S. Lau, C. S. Pai, C. S. Wu, T. F. Kuech and B. X. Liu, Appl. Phys. Lett. 41, 77 (1982).
5. B. Y. Tsaur and L. S. Hung, Appl. Phys. Lett. 38, 626 (1981).
6. K. N. Tu, R. D. Thompson and B. Y. Tsaur, Appl. Phys. Lett. 38, 626 (1981).
7. H. Norde, J. de Sousa Pires, F. d'Heurle, F. Pesavento, S. Petersson and P. A. Tove, Appl. Phys. Lett. 38, 865 (1981).

### Figure Captions

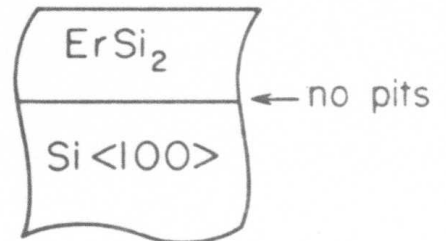
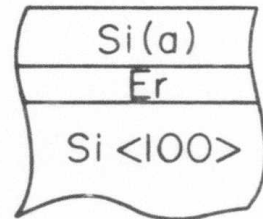
1. Upper portion: Optical micrographs (with Normaski contrast) of top views of  $\text{ErSi}_2$  layers formed by two different methods. Lower portion: Schematic showing  $\text{ErSi}_2$  Schottky barrier contacts formed by conventional method and the new approach.
2. I-V characteristics of  $\text{Er/Si}\langle\text{p},100\rangle$  and  $\text{Si(a)}/\text{Er/Si}\langle\text{p},100\rangle$  diodes before annealing. The diode size is 3 mm in diameter.
3. I-V characteristics of  $\text{Er/Si}\langle\text{p},100\rangle$  and  $\text{Si(a)}/\text{Er/Si}\langle\text{p},100\rangle$  diodes (3 mm in diameter) after annealing at  $450^\circ\text{C}$  for 30 minutes in forming gas.
4. Barrier height vs. annealing temperature (30 minutes annealing time).
5. Barrier height vs. annealing time at  $380^\circ\text{C}$ .



10  $\mu$ m



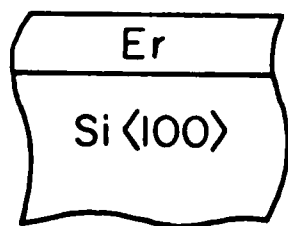
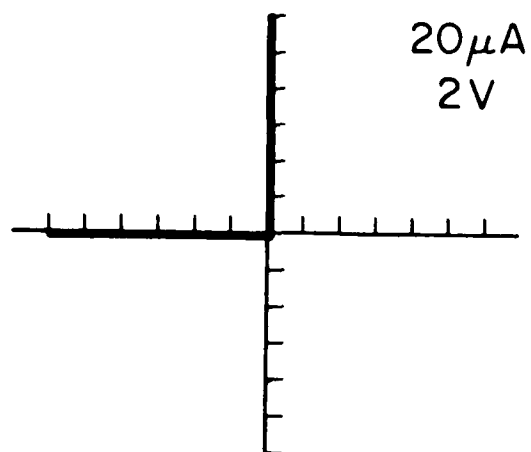
Conventional Method



New Approach

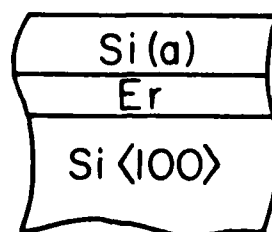
450°C  
30 min

Figure 1



Before Anneal

3mm diodes



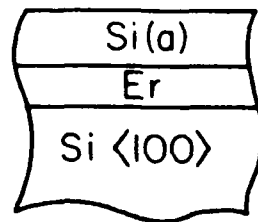
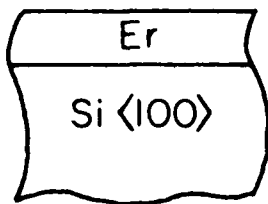
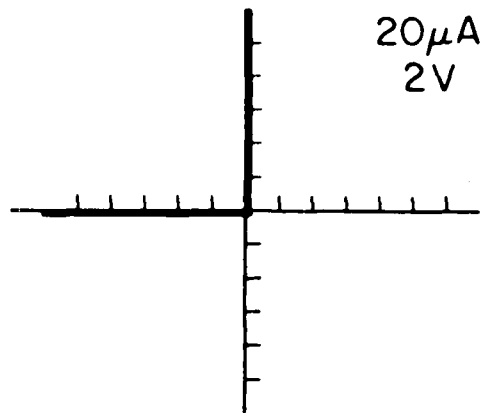
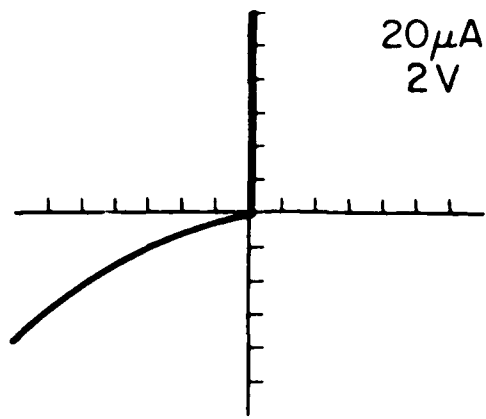
$$\phi_B^p = 0.68 \pm .01 \text{ eV}$$

$$n \approx 1.05$$

$$\phi_B^p = 0.68 \pm .01 \text{ eV}$$

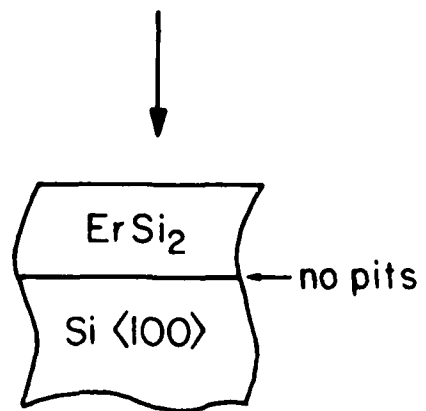
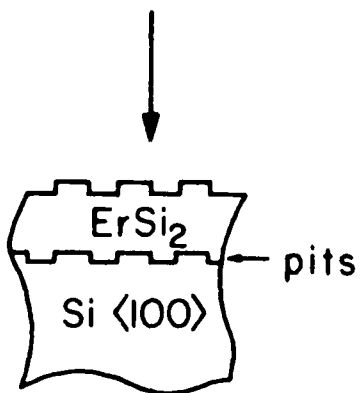
$$n \approx 1.05$$

Figure 2



450°C  
30min

3mm diodes



$$\phi_B^p = 0.70 \pm .02V$$

$$n \approx 1.1$$

$$\phi_B^p = 0.76 \pm .02V$$

$$n \approx 1.05$$

Figure 3

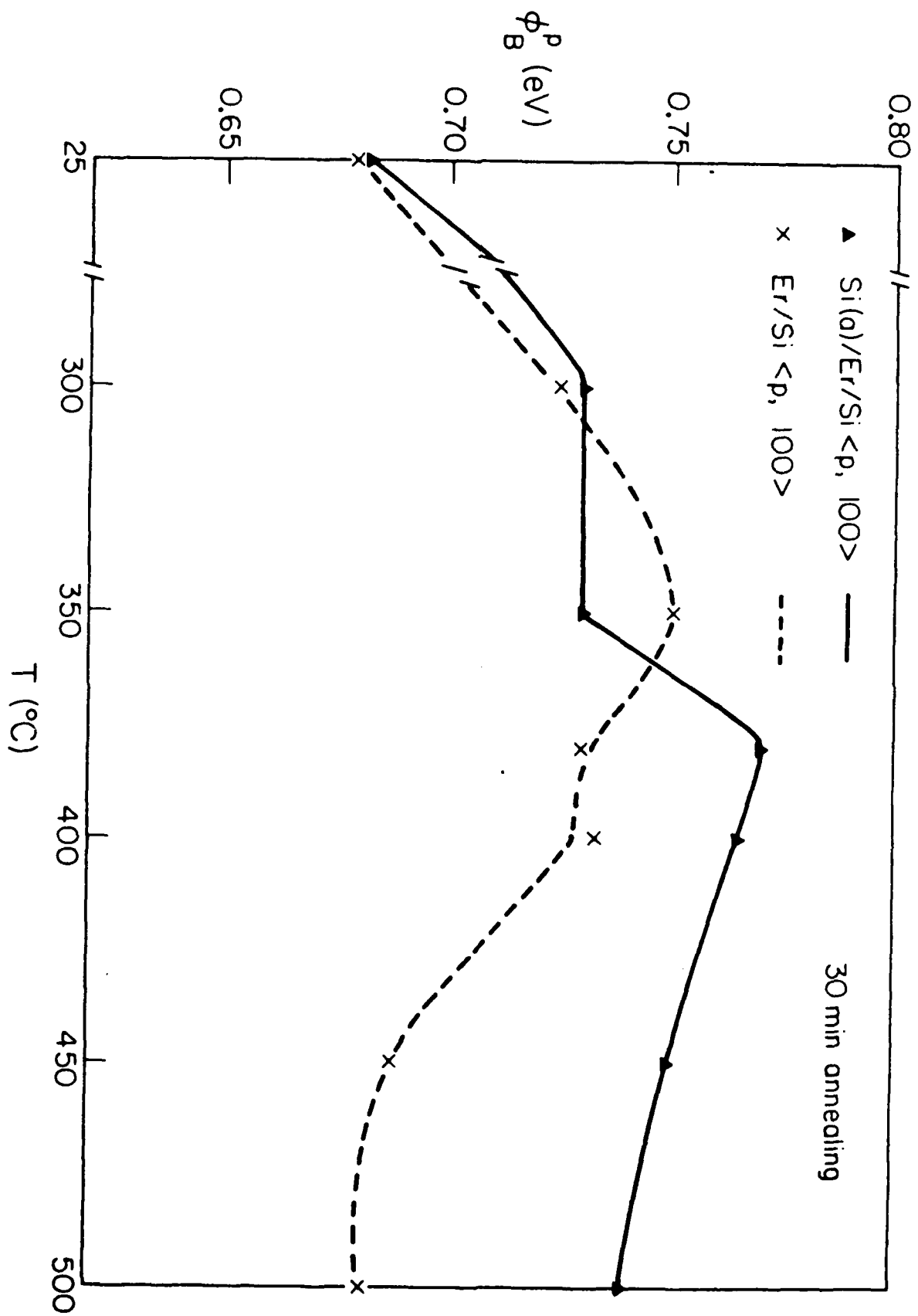


Figure 4

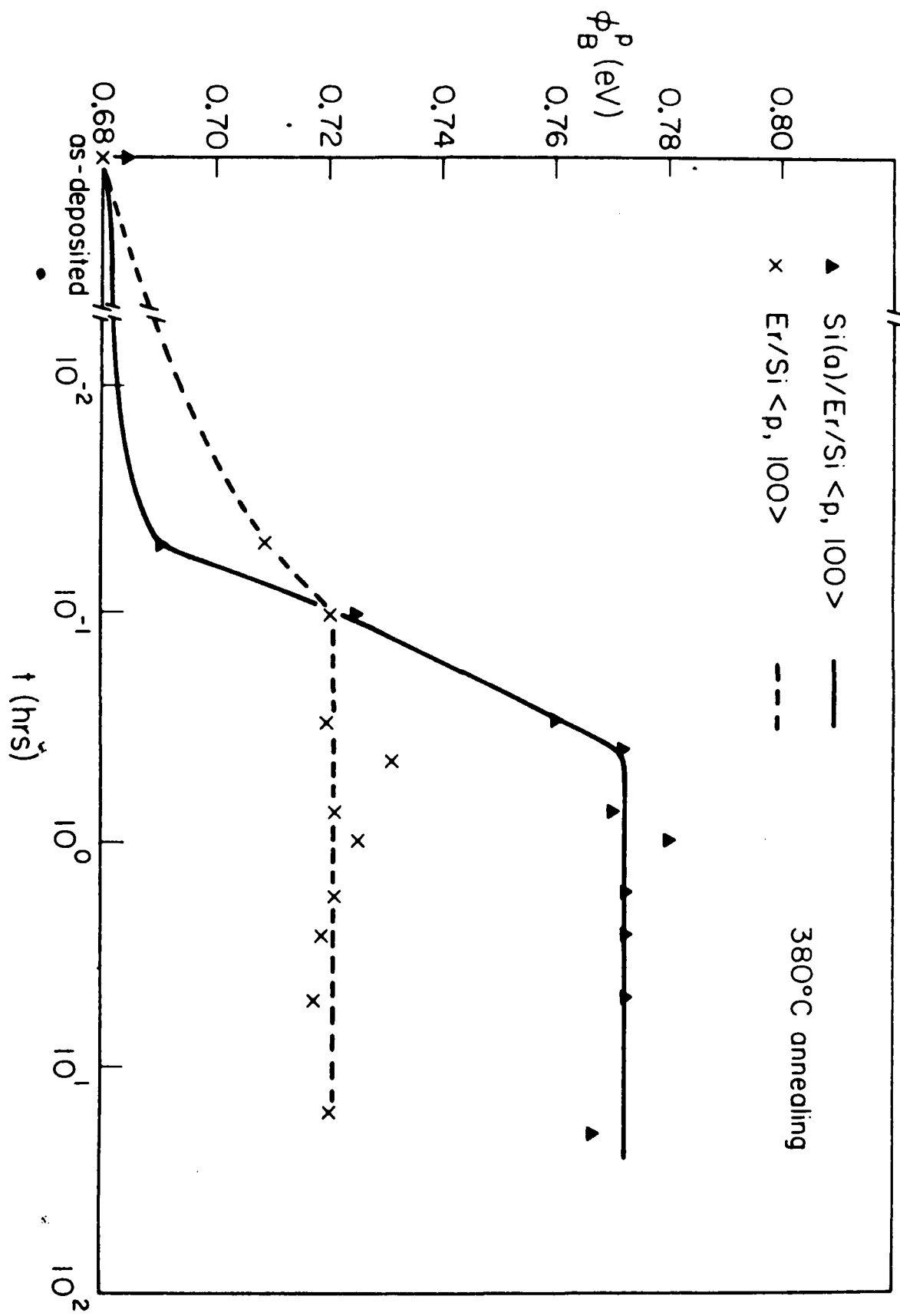


Figure 5